Available online at www.sciencedirect.com
SCIENCE DIRECT®
Applied Surface Science 252 (2006) 3647–3657
applied surface science
www.elsevier.com/locate/apsusc

Vibrational EELS and DFT study of propionic acid and pyruvic acid on Ni(1 0 0): Effects of keto group substitution on room-temperature adsorption and thermal chemistry

X. Yang, Z.H. He, X.J. Zhou, S.H. Xu, K.T. Leung *

Department of Chemistry, University of Waterloo, Waterloo, Ont., Canada N2L 3G1

Received 24 January 2005; accepted 24 May 2005
Available online 1 July 2005

Abstract

The room-temperature adsorption and thermally induced processes of propionic acid and pyruvic acid on Ni(1 0 0) have been investigated by electron energy loss spectroscopy (EELS). Computational vibrational analysis of the optimized bidentate structures for acid–Ni model complexes (involving the organic acid and a Ni atom) has been performed by using the two-layer ONIOM method with the Density Functional Theory and used to interpret the vibrational EELS data. Dehydrogenation of the hydroxyl group is found to result in bonding of the carboxylate group in the propionate and pyruvate adspecies to either a single Ni surface atom in a bidentate configuration or two neighbouring Ni atoms in a bridge configuration. Given the similarities in the total energies and related vibrational frequencies obtained by the calculations in the case of pyruvate adspecies, it is difficult to differentiate the alternate adsorption structure, in which the keto O and hydroxyl O atoms are bonded to a Ni atom in a five-member chelate ring configuration. Furthermore, temperature-dependent EELS studies show that both the propionate and pyruvate adspecies could decompose upon annealing to above 400 K and further dissociate to CO adspecies above 550 K and to C and/or O above 600 K.

Keywords: Electron energy loss spectroscopy; Density Functional Theory; Propionic acid; Pyruvic acid; Ni(1 0 0)

1. Introduction

Surface chemistry of organic acids on (transition) metal surfaces is of special interest to a wide range of practical applications including corrosion [1], heterogeneous catalysis [2,3], and biotechnological manufacturing [4]. Controlling these surface processes require mechanistic understanding of chemisorption at the molecular level. In particular, Ni surfaces have continued to attract attention as a viable and inexpensive alternative to precious metal surfaces such as Pd or Pt for catalytic reactions. The interactions of small organic acids such as formic acid (HCOOH) and acetic acid (CH_3COOH) with single-crystal Ni and other metal and related surfaces (e.g., Cu, Pt, Pd, Fe, and UO_2) have been extensively

* Corresponding author. Tel.: +1 519 8884567x5826; fax: +1 519 7460435.
E-mail address: tong@uwaterloo.ca (K.T. Leung).

0169-4332/$ – see front matter © 2005 Elsevier B.V. All rights reserved.
doi:10.1016/j.apsusc.2005.05.047

investigated by theoretical methods [5,6] and numerous experimental techniques, including low energy electron diffraction (LEED) [1,6,7], Auger electron spectroscopy (AES) [1,7], electron energy loss spectroscopy (EELS) [3,7–10], X-ray photoelectron spectroscopy [1,3], temperature programmed desorption (TPD) [3,8,9,11], infrared spectroscopy (IR) [2,6,12,13], infrared-visible sum frequency generation (SFG) [14], and scanning tunnelling microscopy [6]. These studies show that adsorption of these small organic acids (HCOOH and CH_3COOH) on transition metal surfaces generally involves dehydrogenation of the hydroxyl group (as indicated by the absence of the ν(OH) stretching mode in the 3400–3600 cm^{-1} region) and the formation of three possible surface bonding structures with unidentate, bidentate, and bridge geometries [2,8,9,14]. In the unidentate geometry, the hydroxyl O atom is bonded to a single metal atom, giving rise to both the ν_{as}(COO) asymmetric stretching mode (1550–1670 cm^{-1}) and the ν_s(COO) symmetric stretching mode (1365–1450 cm^{-1}) [2,8]. For the bidentate adsorption structure, both carboxylate O atoms are symmetrically bonded to the same metal atom, resulting in a shift in ν(CO) stretching frequencies (due to the change in the bond order) and the strengthening of the ν_s(COO) mode along with a concomitant weakening of the ν_{as}(COO) mode [2,3,9,10]. The bridge adstructure involves bonding of the two carboxylate O atoms individually to two neighbouring metal atoms, and it is found to exhibit similar vibrational modes as the bidentate adstructure [7,10,12].

In the present work, we focus on the surface chemistry of more complex organic acids, including propionic acid (PPA, CH_3CH_2COOH) and α-keto propionic acid or more commonly called pyruvic acid (PA, $CH_3COCOOH$), on Ni(1 0 0). In particular, PPA represents the next member of the aliphatic carboxylic acid beyond acetic acid for extending the database and for examining the effect of an extended alkyl chain on the surface chemistry of Ni. Only a limited number of studies of PPA on Ni [14,15], Pd [9] and Pt [10] by using TPD, SFG and EELS methods have been reported. For PPA adsorbed on Pd and Pt surfaces, the carboxylate group is bonded to the surface with C_{2v} symmetry [9,10]. Except for the two SFG studies that focussed only on the ethyl group of the PPA adsorbed on Ni(1 0 0) [14] and Ni(1 1 0) [15], no other data is available for directly identifying the bonding between the adsorbed PPA and the Ni substrate atoms. Although PA is structurally similar to PPA, the replacement of the $>CH_2$ group by the keto group (>C=O) in PA is expected to provide additional bonding sites for new chemical reactions possibly involving different adsorption arrangements with the substrate metal atoms. As the primary naturally occurring end-product of the metabolism of glucose in glycolysis in the body, PA has also attracted considerable attention as an athletic performance enhancement and fat loss drug [16–19]. In contrast to the small organic acids, only limited studies have been reported for the interactions between PA and metal (oxide) [20–22]. In particular, Tallman and Leussing determined the stability constants of metal-pyruvate by spectrophotometric techniques [20]. They further suggested that the stable configuration of metal-pyruvate could include the binding of the hydroxyl O (after the loss of the hydroxyl H) and the keto O atoms with a metal ion to form a five-member chelate ring, which is different from the bonding models of metal with other organic acids [9,10]. On the other hand, Devdas et al. collected vibrational spectra of pyruvate adspecies on alumina using inelastic electron tunnelling spectroscopy and Fourier transform IR spectroscopy [21]. Their experimental results showed no interaction between the keto group of the pyruvic acid and the alumina surface, but rather bonding between the carboxylate group resulting from dehydrogenation (of the hydroxyl H) and the alumina surface [21]. In addition, Rochefort et al. reported optimized structures of complexes between an Ni atom and a series of α-dicarbonyl molecules by using Density Functional Theory (DFT), and found in particular that, unlike the Ni pyruvate structures [23], the Ni–pyruvic acid molecular complex (i.e., with the PA molecule intact) with the five-member chelate ring structure to be less stable than the unidentate structure [22]. Because dehydrogenation of the carboxylic acid group (with the formation of pyruvate) is generally expected to occur on transition metal surfaces, the calculation for such Ni–pyruvic acid molecular complexes is, however, not particularly relevant to the present chemisorption study [22]. In the present work, we investigate the chemisorption of PPA and PA on Ni(1 0 0) by vibrational EELS. In order to obtain a better understanding of the mechanism of surface

adsorption of PA on Ni(1 0 0) and the substitutional effect of the $>CH_2$ group (as in PPA) by the keto group (as in PA), we perform DFT calculations to determine the stable carboxylate structures involving a single Ni atom and a dehydrogenated PPA or PA radical. Of particular interest is the thermally induced chemistry of these more complex organic acids on Ni surfaces, which may offer more realistic understanding of the mechanisms of surface reactions used in industrial (catalytic) processes that are often conducted above room-temperature (RT).

2. Experimental details

All the experiments in the present work were conducted in a home-built ultrahigh vacuum (UHV) system, with a base pressure better than 1×10^{-10} Torr, described elsewhere [24,25]. The UHV system was equipped with an ion-sputtering gun, a four-grid retarding-field optics for reverse-view LEED and AES analyses, a differentially pumped 1–300 amu quadrupole mass spectrometer for TPD studies, and a home-built multi-technique electron energy loss spectrometer capable of both electronic and vibrational EELS measurements [26]. Details of our EELS spectrometer has been described in our earlier work [25–27]. All the vibrational EELS experiments were performed with an impact energy of 5 eV and a specular reflection geometry (45° from the surface normal). A routine energy resolution of 12–20 meV (97–160 cm^{-1}) full-width at half-maximum could be achieved with a typical count rate of 100,000–300,000 counts per second for the elastic peak.

The single-crystal Ni(1 0 0) sample (10 mm in diameter and 1 mm thick) with a stated purity of 99.995% and an accuracy of ±1° from the (1 0 0) plane was purchased from Accumet Materials. The sample was mechanically mounted on a Ta sample plate by spot-welding a pair of 0.5 mm thick Ta strips at the edge of the nickel crystal to the sample plate. The Ni crystal was cleaned by repeated cycles of Ar^+ sputtering and annealing to 1000 K until a sharp 1×1 LEED pattern was obtained. The surface cleanliness of the sample was confirmed by a featureless EELS spectrum. Sample annealing was achieved by electron bombardment from a heated W filament at the backside of the Ni sample. The temperature of the sample was monitored by a K-type thermocouple (mechanically fastened to the front side of the sample) with an absolute accuracy of ±20 K. The presence of residual CO (and CO_2) in our UHV chamber could easily lead to contamination on the reactive clean Ni surface, as indicated by the emergence of a strong ν(CO) stretching mode near 1800–2000 cm^{-1} [28] in about 30 min. In order to minimize possible surface contamination, we used circulated liquid nitrogen to reduce the amount of time required to cool the sample back to RT before sample dosing.

Propionic acid (at 99.5% purity) and pyruvic acid (at 98% purity) were purchased from Sigma–Aldrich and degassed by several freeze-pump-thaw cycles prior to use. No discernible impurities could be found in the respective cracking patterns of the chemicals [29] during sample dosing. The exposure (in units of Langmuir, 1 L = 1×10^{-6} Torr s) was controlled by backfilling the UHV chamber to a predetermined chamber pressure (as measured by an uncalibrated ionization gauge) for an appropriate period of time by using a variable leak valve. All the exposures were performed at RT and a saturation exposure was used unless stated otherwise.

3. Results and discussion

3.1. Room-temperature chemisorption of PPA and PA on Ni(1 0 0)

Fig. 1 compares the vibrational EELS spectra for a RT saturation coverage of PPA and that of PA on Ni(1 0 0). The positions of the electron energy loss peaks in the present work were obtained by a non-linear least-square fitting procedure (employing Gaussian–Lorentzian lineshapes for individual EELS features) after appropriate subtraction of a polynomial background. Table 1 summarizes the assignments for typical vibrational frequencies obtained for PPA and PA molecules [30,31] and their corresponding values in salt [23,32] and/or adsorbed forms [10,21]. The PPA/Ni(1 0 0) spectrum (Fig. 1a) is dominated by a strong EELS feature at 2910 cm^{-1}, which could be attributed to the ν(CH) stretching modes in the ethyl group [9,10,14,15,23,30]. The other strong feature at 1405 cm^{-1} could be assigned to a combination of $\delta_{as}(CH_3)$ asymmetric bending and ν_s(COO) symmetric

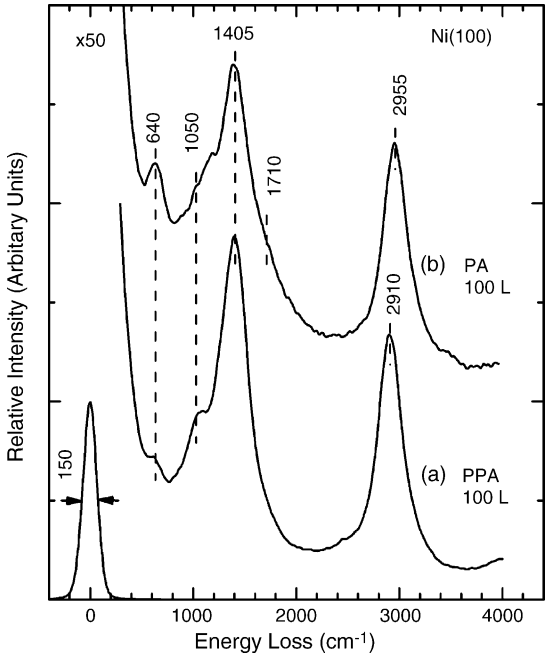

Fig. 1. Vibrational electron energy loss spectra of 100 L exposures of (a) propionic acid (PPA) and (b) pyruvic acid (PA) on Ni(1 0 0) at room-temperature.

stretching modes, which were found to be at 1421 cm^{-1} and 1395 cm^{-1} for (PPA)Ni [23] and PPA/Pt(1 1 1) [10], respectively (Table 1). In accord with the earlier work [10,23] (Table 1), the weak features at 1050 and 640 cm^{-1} could be attributed to the $\gamma(CH_3)$ rocking mode and $\delta_s(COO)$ bending mode, respectively. In comparison with the vibrational features of the liquid-phase PPA [30], the absence of the $\nu(OH)$ stretching mode (at 3100 cm^{-1}) in the EELS spectrum of the adsorbed PPA indicates H evolution from the hydroxyl group upon adsorption on Ni(1 0 0) at RT. Furthermore, the $\nu_{as}(COO)$ asymmetric stretching mode (near 1600 cm^{-1}) of the carboxylate group is also found to be absent in the spectrum (Fig. 1a). The absence of these EELS features together suggests that PPA does not adsorb on Ni(1 0 0) in a unidentate fashion but rather in either the bidentate or bridge bonding configuration [9,10], in which case the $\nu_{as}(COO)$ asymmetric vibration could produce a dipole moment nearly parallel to the surface and become less active in the vibrational spectrum according to the surface selection rules [33]. It should be noted that the EELS spectra of PPA/Pd(1 1 1) reported by Davis and Barteau [9] and PPA/Pt(1 1 1) by Avery [10] are found to be very similar to that for Ni(1 0 0) in the present work, further suggesting a common local adsorption geometry on these metal surfaces. The surface configuration of PPA/Ni(1 0 0) is also found to be similar to that of formic acid and acetic acid on Ni [2,7,8,11,12] and other metal (oxide) surfaces [1,3,6,9], which suggests that the aliphatic carboxylic acids would likely follow the same chemisorption model.

Evidently, the vibrational features for PPA on Ni(1 0 0) (Fig. 1a) are also found in the EELS spectrum of PA on Ni(1 0 0) depicted in Fig. 1b, with the respective assignments shown in Table 1. An additional EELS feature at 1710 cm^{-1} for PA/Ni(1 0 0) is observed and assigned to the $\nu(C{=}O_{keto})$ stretching mode of the keto group, which is in accord with the IR study of PA molecule by Hollenstein et al. [31], (PA)Na by Kiakihana and Okamoto [32] and PA/Al_2O_3 by Devdas et al. [21] (Table 1). It should be noted that the molecular configuration of (PA)Na is found to be different from that of PA/Al_2O_3, whereby the Na atom is located asymmetrically in between the hydroxyl O and the keto O atoms for (PA)Na (in a "pseudo" five-member chelate ring) [34] while both the carboxylate O atoms are bonded to the Al_2O_3 surface in the latter case [21]. It is, therefore, possible that both PA adstructures are viable on Ni(1 0 0) given the similarity between the present EELS data for PA/Ni(1 0 0) and the IR data of both (PA)Na [34] and PA/Al_2O_3 [21]. It is also of interest to note that the feature at 640 cm^{-1} in the PPA/Ni(1 0 0) spectrum (Fig. 1a) is assigned to the $\delta_s(COO)$ symmetric bending mode [10], while the stronger feature at the same frequency in the PA/Ni(1 0 0) spectrum (Fig. 1b) could be assigned to a mixture of $\nu_s(CCC)$ stretching mode, $\gamma(C{=}O_{keto})$ and $\gamma(CH_3)$ rocking modes, in accord with the IR spectra of PA molecule [31] and (PA)Na [32]. Although the feature at 640 cm^{-1} is found to be absent in the IR spectrum of PA/Al_2O_3, we cannot rule out the possible presence of similar configuration on Ni(1 0 0). We therefore hypothesize that PA adsorbs onto Ni(1 0 0) via bonding of either both carboxylate O atoms or the hydroxyl O and keto O atoms.

In order to investigate the local bonding structures of PPA and PA on Ni(1 0 0) especially to clarify the role of the keto group in the adsorption, we have

Table 1
Comparison of experimental vibrational frequencies (in cm^{-1}) for propionic acid (PPA) and pyruvic acid (PA) on Ni(1 0 0) with the respective calculated frequencies for model acid–Ni complexes, and with other literature data[a]

Vibrational modes	PPA liquid [30]	(PPA)Ni [23]	PPA/Pt (1 1 1) [10]	PPA/Ni (1 0 0)	PPA–Ni	PA gas [31]	(PA)Na [32]	PA/Al_2O_3 [21]	PA/Ni (1 0 0)	Tte–Ni	Tce–Ni
ν(OH)	3100	–	–	–	–	~3463	–	3593	–	–	–
$\nu_{as}(CH_3)$	2990	2942			3059	3027	3024	–		3092	3092
$\nu_{as}(CH_2)$ in the CH_3 group	2950	2979			3057	2977	2989	2978	}2955	3040	[3029]
$\nu_s(CH_3)$	}2890	–	}2950	}2910	2985	2932	2932	2935		[2981]	[2977]
$\nu_s(CH_2)$		–			2969	–	–	–	–	–	–
$\nu_{as}(CH_2)$	–	–			[2993]	–	–	–	–	–	–
ν_{as}(COO)	1714	1569	–	–	2132	1805	1633	1604	–	1496	1679
$\nu(C{=}O_{keto})$	–	–	–	–	–	1733	1709	1760	1710	1730	1583
$\delta_{as}(CH_3)$	1464	1467	–	–	[1496], [1480]	–	1406	–	}1405	1433	1419
$\delta_{as}(CH_3)$, ν_s(COO)	–	1421	1395	1405	1623	1422, 1390	1426, 1406	1450		1435, 1368	1422
$\delta_{as}(CH_2)$	1413	–	–	–	1431						
$\delta_s(CH_3)$, δ(COH)[b]	1380	1377	1310	–	[1389]	1360	1354	1372, 1290	–	1351	1358
$\delta(CH_2)$	1335, 1322	1309	–	–	[1269], [1098]	–	–	–	–	–	–
$\gamma(CH_2)$, $\gamma(CH_3)$	1288	1245	–	–	1287	–	–	–	–	–	–
ν(CO)	1235	–	–	–	–	–	–	–	–	–	–
$\gamma(CH_3)$, ν_s(CCC), $\delta(C{=}O_{keto})$[c], δ(COH)[b]	–	–	–	–	–	1218, 1204	1188	1211, 1158	–	–	1226
ν(CC), $\gamma(CH_3)$	1076	1092	}1090	}1050	[1059]	1134	–	1095	}1050	1144	1164
$\gamma(CH_3)$, γ(CCC), $\gamma(C{=}O_{keto})$[c]	1005	988				1021	1018	1054		1003	978
$\gamma(CH_3)$	990	–	–	–	[979]	~970	982	941	–	937	953
γ(COH)	930	–	–	–	–						
ν(CC), δ_s(COO)	844	895	–	–	[791]	761	834	817	–	822	788
$\gamma(CH_2)$, $\gamma(CH_3)$	808	813	–	–	[787], [473]	–	–	–	–	–	–
γ(COO), $\gamma(CH_3)$, γ(COH)[b]	–	–	–	–	–	668	750	776	780	663	685
$\gamma(C{=}O_{keto})$, ν_s(CCC), $\gamma(CH_3)$	–	–	–	–	–	604	631	–	640	608	620
δ_s(COO)	650	–	660	640	[584]						
δ(CCC), δ(COO), $\gamma(CH_3)$	494, 305	–	–	–	503	–	546	428	–	502, 437	[511], [487]
γ(COO), $\gamma(CH_3)$, $\gamma(C{=}O_{keto})$[c]	600	–	–	–	–	392	432	256	–	421	340
ν_{as}(NiOO)	–	–	270	–	[353], [276]	–	–	–	–	299, 138	321
δ(CCC), δ(COO), $\delta(C{=}O_{keto})$						–	396, 299	–	–	–	–
ν_s(NiOO), δ(CCC)										268	276
$\gamma(CH_3)$, $\gamma(CH_2)$[d]	–	–	–	–	[164]	134	–	–	–	[103]	68
γ(CCC), $\gamma(CH_3)$, $\gamma(CH_2)$[d]	–	–	–	–	[138], [100]	90	–	–	–	112	138
γ(NiOO)	–	–	–	–	[129]						
$\gamma(CH_3)$, γ(COO)						–	–	–	–	34	[101]

[a] *Legends:* ν, stretch; δ, bend; γ, rock; s, symmetric; as, asymmetric. For weak features with relative intensities less than 1%, the corresponding calculated vibrational frequencies are listed in parentheses.

[b] OH related features observed only in the PPA (liquid-phase) and PA (gas-phase) molecules.

[c] Keto group related features observed only in the gaseous PA and (PA)Na samples.

[d] CH_2 related features observed only in the PPA–Ni complex.

calculated the total energies, equilibrium geometries and the corresponding harmonic vibrational frequencies of plausible configurations of the acids bonded to a single Ni atom by using a hybrid DFT method at the BLYP (Becke's one-parameter hybrid functional with the Lee–Yang–Parr correlation functional) level [35,36]. The calculations were performed by using the GAUSSIAN 98 suite of programs [37] at a home-built technical computer farm based on the Pentium-4 technology. The two-layered ONIOM method [38,39] was used with the Ni atom in the lower layer and the other atoms (of the acid) in the top layer. The LANL2DZ basis set (which employs the Dunning–Huzinaga double zeta basis set for the 18 outermost electrons [40] and the effective core potentials of Hay and Wadt for all the other electrons [41]) was used for the Ni atom, while the 6-31G** basis set was used for the atoms in the top layer (acid). Although no basis set superposition error has been included in the calculation, the zero-point vibrational energy corrections were performed in the present calculation for the total energies for the acid–Ni complexes. Fig. 2 compares the equilibrium structures of a free PPA molecule and the three stable conformers of PA as discussed in our earlier work [19]. It should be noted that even though our earlier computation was performed at the B3LYP/6-311++G(3df,3pd) level, the results for the structures are found to be nearly identical to those obtained at the BLYP/6-31G** level used in the present work. The total energies of free PPA and PA molecules obtained at the BLYP/6-31G** level in the present work are also listed in hartree atomic units (A.U.) in Fig. 2. The notation for the PA monomer conformers has been discussed elsewhere [19]. Briefly, the dihedral angle C_{methyl}–C_{keto}–C_{acid}–$O_{hydroxyl}$ of 0° and 180° is labelled by an upper-case letter C (for the *cis* form) and T (for the *trans* form), respectively, while the dihedral angle C_{keto}–C_{acid}–O–H of 0° and 180° is labelled by a lower-case letter c (for the *cis* form) and t (for the *trans* form), respectively. Only the more stable eclipsed orientation of the methyl group with respect to the keto group (i.e., with the corresponding dihedral angle H_{methyl}–C_{methyl}–C_{keto}=O_{keto} of 0°) is considered here and is denoted by a lower-case letter e. Except for the difference in the $>CH_2$ group and the keto group, the molecular backbone (C_{methyl}–C–C_{acid}OO) of the PPA (Fig. 2a) is essentially the same as that of PA (Fig. 2b–d). Interestingly, the Tce structure (with the hydroxyl group pointing towards the keto O, Fig. 2d) is more stable than the Tte structure (with the hydroxyl group directed away from the keto O, Fig. 2b), which is similar to the PPA structure with the same carboxylic acid group arrangement (Fig. 2a). Furthermore, the structures for the free molecules are also compared with their corresponding PPA–Ni (Fig. 2e) and PA–Ni complexes (Fig. 2f and g), in which the hydroxyl H atom is replaced by the Ni atom. It should be noted that structure optimization and vibrational frequency analysis have been performed with both C_s and C_1 symmetries for all the acid–Ni complexes in the present work. An imaginary frequency was found in the calculated C_s structure for PPA–Ni, which indicates that the PPA–Ni complex with C_s symmetry does not correspond to a local minimum in the potential energy surface at the BLYP level. Only the C_1 structure of the PPA–Ni complex is therefore considered in the present work. In the case of the three PA–Ni complexes: Tte–Ni (Fig. 2f), Cte–Ni (same as Tte–Ni, see later) and Tce–Ni (Fig. 2g), the calculation shows nearly identical total energies without any imaginary frequency for both C_1 and C_s symmetries (with energy difference less than 0.3 kJ/mol). We therefore consider only the results obtained with C_s symmetry for PA–Ni in the present work. It is also of interest to note that the calculated geometries, total energies and vibrational frequencies for both Tte–Ni and Cte–Ni complexes are found to be essentially identical, as expected from the same configuration resulting from the loss of the hydroxyl H atom in both the Tte and Cte structures (with nearly degenerate total energies, Fig. 2b and c). Only the calculated results for the Tte–Ni complex are therefore listed in the present work. The aforementioned calculated structures correspond to what we refer to as bidentate configurations. As more extensive calculations involving more than one Ni atom are beyond the scope of the present work, we show in Fig. 2 "hypothetical" bonding geometries for the respective bridge configurations of PPA and both PA Tte and Tce conformers on Ni(1 0 0). Because the bidentate and bridge configurations in effect differ from each other by half a Ni–Ni spacing from the commensurate bonding positions, we do not expect significant changes in most of the vibrational modes of the adsorbates. Furthermore, it is difficult to differentiate these two configurations experimentally due to

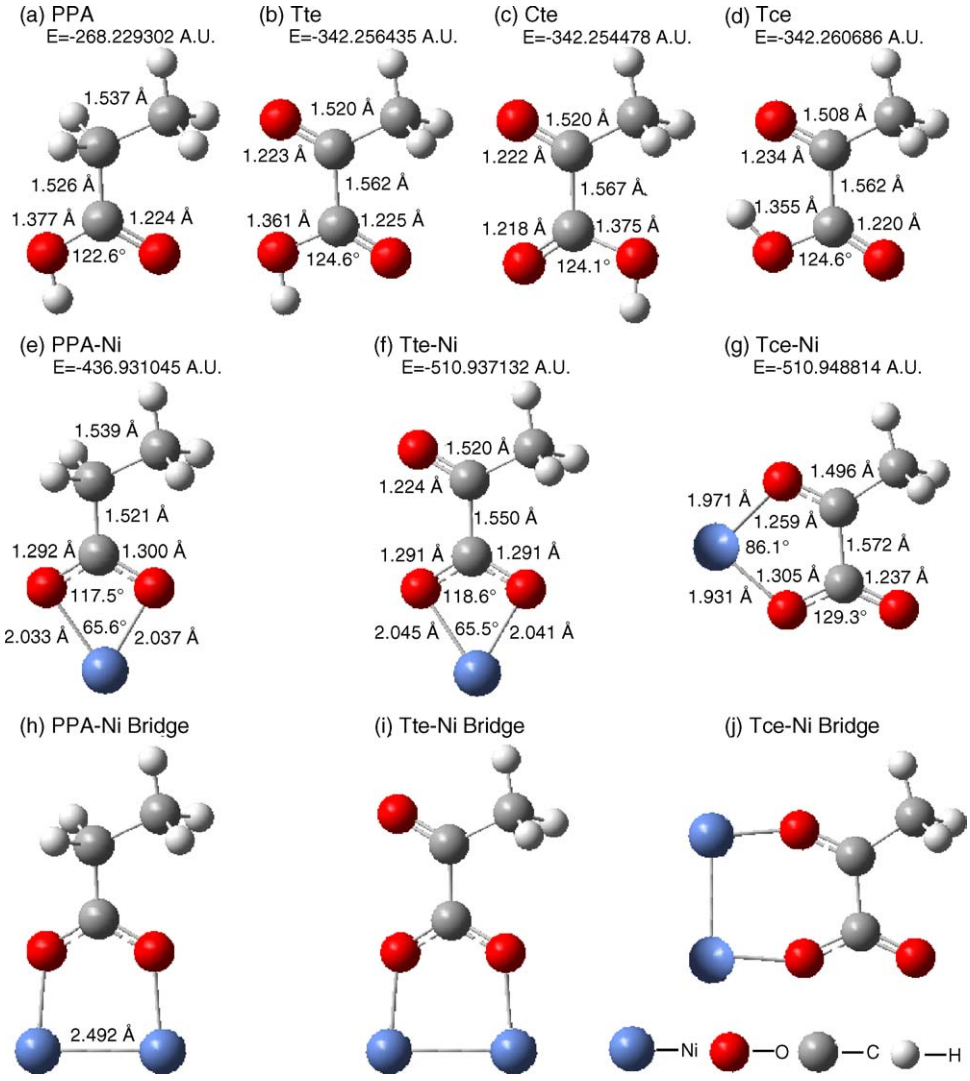

Fig. 2. Equilibrium configurations of (a) free propionic acid (PPA) and different conformers of pyruvic acid (PA): (b) Tte, (c) Cte and (d) Tce, and their corresponding complexes with a single Ni atom: (e) PPA–Ni (f) Tte–Ni and (g) Tce–Ni, all calculated by using Density Functional Theory as discussed in text. The corresponding total energies in atomic units (AU) are also indicated. Hypothetical complexes involving bridge bonding arrangements with two Ni atoms are shown schematically as (h) PPA–Ni bridge, (i) Tte–Ni bridge and (j) Tce–Ni bridge.

the low frequencies expected for the Ni-related vibrations.

Fig. 2 also indicates the primary structural parameters of the equilibrium structures (including the C–C bond lengths in the C–C–C backbone and the C–O bond length of the keto group) as well as the corresponding bond angle of the carboxylate group ($\angle$OCO) and the two Ni–O bond lengths of the acid–Ni complexes. Evidently, bonding of the PPA and that of the PA Tte conformer to the Ni atom compress the respective bond angles of the carboxylate group ($\angle$OCO) by 5–6° (Fig. 2a–c, e and f). The corresponding C–O bond lengths in the carboxylate group are found to be in between those of C=O and C–O in the carboxylic acid group and are consistent with a bond order of 1.5. Furthermore, bonding with the Ni atom does not appear to affect the other structural parameters (e.g., the bond lengths in the C–C–C

backbone) and correspondingly no notable differences are observed in their respective vibrational frequencies (Table 1). In the case of the PA Tce–Ni complex, the Ni atom is bonded to both the keto O and the hydroxyl O atoms to form a five-member chelate ring (Fig. 2g), which appears to open up the ∠OCO bond angle of the carboxylate group by ~5°.

Of special interest to the present work is the effect of replacing the $>CH_2$ in the PPA–Ni complex (Fig. 2e) by the keto group in the PA Tte–Ni complex (Fig. 2f) on the vibrational modes involving the carboxylate group. In particular, notable differences in the frequencies are found in the stretching modes of COO in the two complexes (with the strongest intensity) (Table 1), which reflects the effects of $>CH_2$ and >C=O (keto) ligands on the respective carboxylate groups. On the other hand, the corresponding COO bending modes and Ni–O stretching modes appear to be quite similar (Table 1), which suggests that Ni predominates the contributions to the dipole moments in these vibrational modes. In the case of the PA–Ni complexes involving the Tte and Tce conformers, minor difference in the frequency of the ν_{as}(COO) asymmetric stretch is observed while the other Ni-bonding related modes remain essentially unchanged. However, it is generally difficult to predict the effects of two rather different structures of the conformers in the PA–Ni complexes on the aforementioned vibrational modes.

Table 1 also compares the calculated vibrational frequencies of the acid–Ni complexes with the available data on similar systems and with the experimental data obtained in the present work. Evidently, the calculated frequencies for the ethyl group including the stretching modes from 2969 to 3059 cm^{-1}, bending modes at 1431 cm^{-1} and rocking modes at 1287 cm^{-1} for PPA–Ni are found to be in good accord with the earlier results for PPA [30], (PPA)Ni [23] and PPA/Pt(1 1 1) [10] as well as with the present experimental data (Table 1). On the other hand, the calculated ν_{as}(COO) stretching mode at 2132 cm^{-1} is considerably higher in frequency than that for both the PPA and the (PPA)Ni (Table 1). This feature is, however, not observed in the present experimental spectrum (Fig. 1a), which is consistent with our proposal that the PPA molecule bonds to Ni(1 0 0) via the bidentate or bridge configuration. The weak ν_{as}(NiOO) asymmetric stretching modes at 353 and 276 cm^{-1} in the calculated spectrum of PPA–Ni could not be discerned in the experimental spectrum (Fig. 1a) due to the limited instrumental resolution.

In the case of the PA–Ni complexes, the vibrational frequencies of the CH_3 group for both Tte and Tce conformers (Table 1) are found to be in good agreement with those of the PA molecule [31], (PA)Na [32], and PA/Al_2O_3 [21], and with the present data for PA/Ni(1 0 0), which confirms that the methyl group is not directly involved in the chemisorption. Furthermore, the total energy for the PA Tce–Ni complex (Fig. 2g) is found to be lower by 30.67 kJ/mol than that for the PA Tte–Ni complex (Fig. 2f), which suggests that the five-member chelate ring in the Tce–Ni complex (Fig. 2g) provides a more stable bonding geometry for PA on Ni(1 0 0). On the other hand, the PA Tce–Ni configuration would have the dipole moment for the ν_s(COO) symmetric stretching mode oriented near parallel to the surface, in contrast to the vertical dipole moment orientation for the PA Tte–Ni case. We therefore cannot rule out the PA Tte–Ni adsorption structure because of the strong ν_s(COO) symmetric stretching mode observed at 1405 cm^{-1} in the experimental spectrum (Fig. 1b). Moreover, the presence of the vibrational feature at 1710 cm^{-1} in the experimental spectrum (Fig. 1b), previously assigned to the ν(C=O_{keto}) stretching mode in PA [31] and (PA)Na [32], also correlates well with the calculated spectra for both the PA Tte–Ni and Tce–Ni complexes, except for the different assignments [ν(C=O_{keto}) stretching mode at 1730 cm^{-1} for PA Tte–Ni (Fig. 2f) and ν_{as}(COO) asymmetric stretching mode at 1679 cm^{-1} for PA Tce–Ni (Fig. 2g)] (Table 1). It is therefore quite plausible that the Tce–Ni and Tte–Ni configurations could both be present in the case of PA adsorption on Ni(1 0 0). Furthermore, given the aforementioned ambiguity between the bidentate and bridge bonding configurations, the present EELS spectrum supports the presence of both Tte–Ni (Fig. 2f and i) and Tce–Ni (Fig. 2g and j) as the local bonding structures for PA on Ni(1 0 0) in both bidentate and bridge configurations.

3.2. Thermal evolution of PPA and PA on Ni(1 0 0)

The effects of annealing the PPA/Ni(1 0 0) and PA/Ni(1 0 0) samples are shown in Figs. 3 and 4,

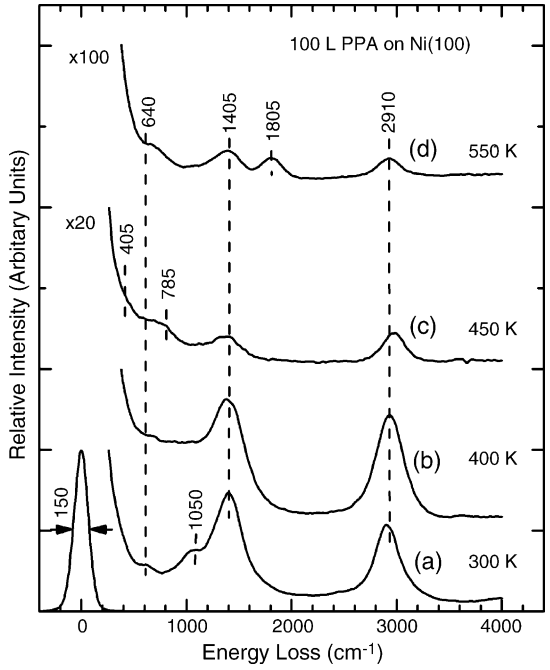

Fig. 3. Vibrational electron energy loss spectra for 100 L exposure of propionic acid (PPA) on Ni(1 0 0) (a) at 300 K, followed by annealing to (b) 400 K, (c) 450 K and (d) 550 K.

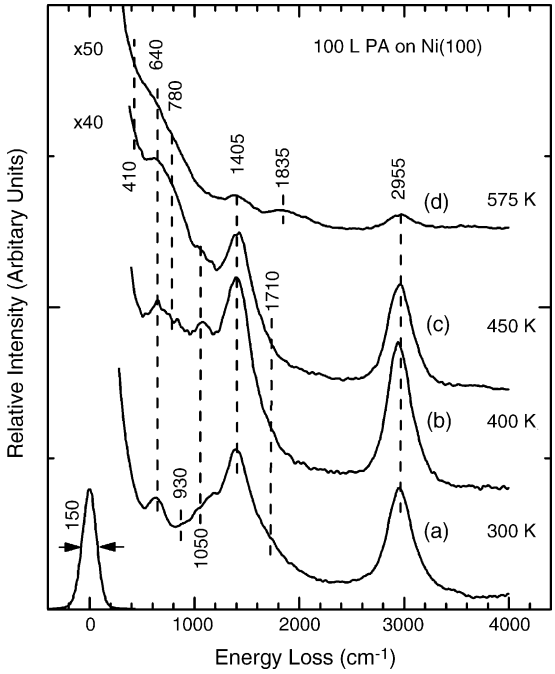

Fig. 4. Vibrational electron energy loss spectra for 100 L exposure of pyruvic acid (PA) on Ni(1 0 0) (a) at 300 K, followed by annealing to (b) 400 K, (c) 450 K and (d) 575 K.

respectively. Evidently, the intensities of the vibrational features correlated with the ethyl group at 2910 cm^{-1} (stretching modes), 1405 cm^{-1} (bending modes) and 1050 cm^{-1} (rocking modes) are found to increase slightly upon annealing from 300 to 400 K, which is likely caused by partial ordering of the adspecies that leads to increase in the specular reflectivity. Upon further annealing from 400 to 450 K, considerable reductions are observed in the intensities of the ethyl group related features but not in that of the δ_s(COO) symmetric bending feature at 640 cm^{-1} (Fig. 3b and c), which suggests decomposition of the adsorbed PPA and/or partial molecular desorption above 400 K. Similar thermal evolution behaviour has also been observed in the TPD/SFG study of PPA/Ni(1 1 0) by Yuzawa et al. [15], which shows that the adsorbed PPA undergoes thermal decomposition above 390 K. The presence of the ν(Ni–O) stretching mode at 405 cm^{-1} [7] and a broad feature at 785 cm^{-1} also becomes more evident upon annealing to 450 K (Fig. 3c). The broad feature at 785 cm^{-1} could be attributed to the δ(CH) out-of-plane bending mode of acetylide (−C≡CH) species resulting from thermal decomposition of the dissociated PPA fragments, as was previously proposed for the adsorption of PPA on Pd(1 1 1) by Davis and Barteau [9]. Further annealing the sample to 550 K greatly reduces the intensities of the existing vibrational features at 785, 1405 and 2910 cm^{-1} (Fig. 3d), suggesting desorption of the respective hydrocarbon fragments. Moreover, the emergence of a weak vibrational band at 1805 cm^{-1} (Fig. 3d) is clearly evident, which could be assigned to ν(C–O) stretch of chemisorbed CO fragments at bridge sites [3,9,28] arising from thermal dissociation of the carboxylate group on Ni(1 0 0) at 550 K. In contrast to PPA (and acetic acid) on Pd(1 1 1) that was found to decompose at RT upon adsorption at 170 K [9], the adsorbed PPA species on Ni(1 0 0) (this work) and Ni(1 1 0) [15] are found to be relatively more stable, with thermal decomposition into smaller species evidently occurring above 400 K. Finally, all the vibrational features are found to extinguish upon annealing to 600 K (not shown). After leaving the sample overnight, the

resulting EELS spectrum evidently remained unchanged, which suggests that the Ni(1 0 0) surface was passivated likely by C or O atoms that were produced by the overall thermal decomposition process to 600 K.

Similar to the thermal evolution of PPA/Ni(1 0 0) (Fig. 3), annealing the PA/Ni(1 0 0) sample to 400 K (Fig. 4a and b) is also found to sharpen the CH_3 related vibrational features at 2955, 1405 and 1050 cm^{-1}, likely due to an increase in the surface ordering and therefore reflectivity of the sample. As with the PPA/Ni(1 0 0) sample (Fig. 3c), further annealing the PA/Ni(1 0 0) sample to 450 K (Fig. 4c) and to 575 K (Fig. 4d) appears to reduce and eventually diminish the intensities of the aforementioned CH_3 related vibrational modes, respectively. In contrast, the intensity of the γ(C=O) rocking mode of the keto group at 640 cm^{-1} and that of the corresponding ν(C—O) stretching mode are found to decrease notably to a lesser extent, which suggests that partial dissociation of the PA adspecies is the dominant process over this temperature range. Moreover, the emergence of the feature at 780 cm^{-1}, characteristic of the γ(COO) rocking mode [21,32], from 400 K (Fig. 4b) to 450 K (Fig. 4c) indicates decomposition of the adsorbed PA. Upon further annealing to 575 K (Fig. 4d), the feature at 780 cm^{-1} is almost completely removed while a new feature at 1835 cm^{-1} that is characteristic of ν(CO) stretch of chemisorbed CO (in a bridge site [28]) becomes evident, which therefore suggests further decomposition of the carboxylate group into CO fragments. As with the PPA/Ni(1 0 0) sample, further annealing the PA/Ni(1 0 0) sample to 600 K also totally removes all the vibrational features, and the resulting spectrum remains unchanged overnight indicating that the Ni(1 0 0) surface has been passivated by dissociated C and/or O atoms.

It should be noted that the reduction in the intensities of the CH_3 (and CH_2) and other related features over the 300–450 K range for both organic acids on Ni(1 0 0) does not necessarily rule out the molecular desorption pathway, even though the breakage of two Ni–O bonds (each with a typical bond strength of 391.6 kJ/mol) would be expected to be less favourable than breaking a C–C bond (with a bond strength of 607 kJ/mol) in the adspecies [42].

4. Concluding remarks

In the present work, the room-temperature adsorption of an saturated coverage of PPA and of PA on Ni(1 0 0) and the resulting bonding arrangements have been investigated by using specular-reflection vibrational electron energy loss spectroscopy. Both organic acids are found to undergo dehydrogenation of the hydroxyl group upon bonding of the carboxylate group to Ni(1 0 0) in a bidentate or bridge configuration, in good accord with the earlier studies on, e.g., PPA/Pt(1 1 1) [10] and PA/Al_2O_3 [21]. In the case of PA/Ni(1 0 0), it is not possible to rule out the formation of a five-member chelate ring via bidentate or bridge bonding of the keto O and hydroxyl O atoms with a Ni substrate atom on Ni(1 0 0) based on the EELS spectrum alone. The bonding configurations have been further investigated by computational studies using the DFT ONIOM method with simplified acid–Ni complexes used as the model systems. Vibrational analysis of the model PA–Ni complex for both the Tte–Ni and Tce–Ni geometries shows generally good agreement with the present EELS data and further confirms the plausibility of the proposed bidentate and/or bridge bonding configurations. These calculations also show that the equilibrium structures for both PA Tte–Ni and PA Tce–Ni are energetically stable, while the formation of a five-member chelate ring in the Tce–Ni complex appears to give a lower total energy than that of the Tte–Ni bidentate model complex. Although the calculations involving more than one Ni atom are beyond the scope of the present work, the Tte–Ni complex could also generate a five-member ring structure in a bridge configuration (Fig. 2i), and further calculations would be of interest to determine which types of chelate rings are more stable. The effects of thermal annealing on both organic acids adsorbed on Ni(1 0 0) have also been studied, and the EELS results show that both the propionate and pyruvate adspecies have likely been decomposed above 400 K. Further annealing evidently would cause the adsorbed fragments to undergo further dissociation to CO above 550 K and to C and/or O atoms above 600 K. Our present temperature-dependent EELS study, however, cannot rule out the molecular desorption channel (along with the observed dissociation pathway). Other collaborative techniques such as temperature programmed deso-

rption would be of great interest to further elucidate the thermal chemistry of these intricate organic acid systems on Ni(1 0 0).

Acknowledgements

This work was supported by the Natural Sciences and Engineering Research Council of Canada.

References

[1] S.V. Chong, H. Idriss, Surf. Sci. 504 (2002) 145.
[2] E.W. Scharpf, J.B. Benziger, J. Phys. Chem. 97 (1987) 5531.
[3] R.D. Haley, M.S. Tikhov, R.M. Lambert, Catal. Lett. 76 (2001) 125.
[4] S. Berchmans, P.J. Thomas, C.N.R. Rao, J. Phys. Chem. B 106 (2002) 4647.
[5] J.R.B. Gomes, J.A.N.F. Gomes, Surf. Sci. 432 (1999) 279.
[6] S.M. York, S. Haq, K.V. Kilway, J.M. Philips, F.M. Leibsle, Surf. Sci. 522 (2003) 34.
[7] T.S. Jones, M.R. Ashton, N.V. Richardson, J. Chem. Phys. 90 (1989) 7564.
[8] R.J. Madix, J.L. Gland, G.E. Mitchell, B.A. Sexton, Surf. Sci. 125 (1983) 481.
[9] J.L. Davis, M.A. Barteau, Langmuir 5 (1989) 1299.
[10] N.R. Avery, J. Vac. Sci. Technol. 20 (1982) 592.
[11] J.B. Benziger, R.J. Madix, Surf. Sci. 79 (1979) 394.
[12] S. Haq, J.G. Love, H.E. Sanders, D.A. King, Surf. Sci. 325 (1995) 230.
[13] A. Yamakata, J. Kubota, J.N. Kondo, C. Hirose, K. Domen, F. Wakabayashi, K. Tamaru, Surf. Sci. 433–435 (1999) 210.
[14] T. Yuzawa, T. Shioda, J. Kubota, K. Onda, A. Wada, K. Domen, C. Hirose, Surf. Sci. 416 (1998) L1090.
[15] T. Yuzawa, J. Kubota, K. Onda, A. Wada, K. Domen, C. Hirose, J. Mol. Struct. 413 (1997) 307.
[16] P.E. Hintze, S. Aloisio, V. Vaida, Chem. Phys. Lett. 343 (2001) 159.
[17] A.J.L. Cooper, J.Z. Ginos, A. Meister, Chem. Rev. 83 (1983) 321.
[18] J. Sherman, D. Luciano, A.J. Vander, Human Physiology: The mechanisms of body functions, seventh ed., WCB McGraw-Hill, New York, 1998.
[19] X. Yang, G. Orlova, X.J. Zhou, K.T. Leung, Chem. Phys. Lett. 380 (2003) 34.
[20] D.E. Tallman, D.L. Leussing, J. Am. Chem. Soc. 91 (1969) 6253.
[21] S. Devdas, R.R. Mallik, R. Coast, P.N. Henriksen, Surf. Sci. 326 (1995) 327.
[22] A. Rochefort, P. McBreen, J. Phys. Chem. A 105 (2001) 1320.
[23] R.I. Bickley, H.G.M. Edwards, R. Gustar, S.J. Rose, J. Mol. Struct. 248 (1991) 237.
[24] D.Q. Hu, C.D. MacPherson, K.T. Leung, Solid State Commum. 78 (1991) 1077.
[25] H. Yu, D.Q. Hu, K.T. Leung, J. Vac. Sci. Technol. A 15 (1997) 2653.
[26] D.Q. Hu, Ph.D. Thesis, University of Waterloo, Waterloo, 1993.
[27] H. Yu, K.T. Leung, Surf. Sci. 432 (1999) 245.
[28] N. Vasquez, A.J. Muscat, R.J. Madix, Surf. Sci. 301 (1994) 83.
[29] Wyandotte-ASTM Punched Card Project, Index of Mass Spectral Data, listed by molecular weight and the four strongest peaks, first ed., American Society for Testing and Materials, Philadelphia, 1963.
[30] R.J. Jakobsen, Y. Mikawa, J.R. Allkins, G.L. Carlson, J. Mol. Struct. 10 (1971) 305.
[31] H. Hollenstein, F. Akermann, H.H. Gunthard, Spectrochim. Acta 34A (1978) 1041.
[32] M. Kiakihana, M. Okamoto, J. Phys. Chem. 88 (1984) 1797.
[33] H. Ibach, D.L. Mills, Electron Energy Loss Spectroscopy and Surface Vibrations, Academic, New York, 1982.
[34] S.S. Tavale, L.M. Pant, A.B. Biswas, Acta Cryst. 14 (1961) 1281.
[35] A.D. Becke, Phys. Rev. A38 (1988) 3098.
[36] C. Lee, W. Yang, R.G. Parr, Phys. Rev. B37 (1988) 785.
[37] M.J. Frisch, G.W. Trucks, H.B. Schlegel, G.E. Scuseria, M.A. Robb, J.R. Cheeseman, V.G. Zakrzewski, J.A. Montgomery, R.E. Stratmann, J.C. Burant, S. Dapprich, J.M. Millam, A.D. Daniels, K.N. Kudin, M.C. Strain, O. Farkas, J. Tomasi, V. Barone, M. Cossi, R. Cammi, B. Mennucci, C. Pomelli, C. Adamo, S. Clifford, J. Ochterski, G.A. Petersson, P.Y. Ayala, Q. Cui, K. Morokuma, D.K. Malick, A.D. Rabuck, K. Raghavachari, J.B. Foresman, J. Cioslowski, J.V. Ortiz, B.B. Stefanov, G. Liu, A. Liashenko, P. Piskorz, I. Komaromi, R. Gomperts, R.L. Martin, D.J. Fox, T. Keith, M.A. Al-Laham, C.Y. Peng, A. Nanayakkara, C. Gonzalez, M. Challacombe, P.M.W. Gill, B.G. Johnson, W. Chen, M.W. Wong, J.L. Andres, M. Head-Gordon, E.S. Replogle, J.A. Pople, Gaussian 98 (Revision A.9), Gaussian Inc., Pittsburgh, PA, 1998.
[38] S. Humbel, S. Sieber, K. Morokuma, J. Chem. Phys. 105 (1996) 1959.
[39] M. Scensson, S. Humbel, R.D.J. Froese, T. Matsubara, S. Sieber, K. Morokuma, J. Phys. Chem. 100 (1996) 19357.
[40] T.H. Dunning Jr., P.J. Hay, in: H.F. Schaefer, III (Ed.), Modern Theoretical Chemistry, vol. 3, Plenum, New York, 1976, p. 1.
[41] P.J. Hay, W.R. Wadt, J. Phys. Chem. 82 (1985) 299.
[42] R.C. Weast, Handbook of Chemistry and Physics, 62nd ed., CRC Press Inc., Boca Raton, FL, 1981.